Joule

CellPress

Article

Wind power production from very large offshore wind farms

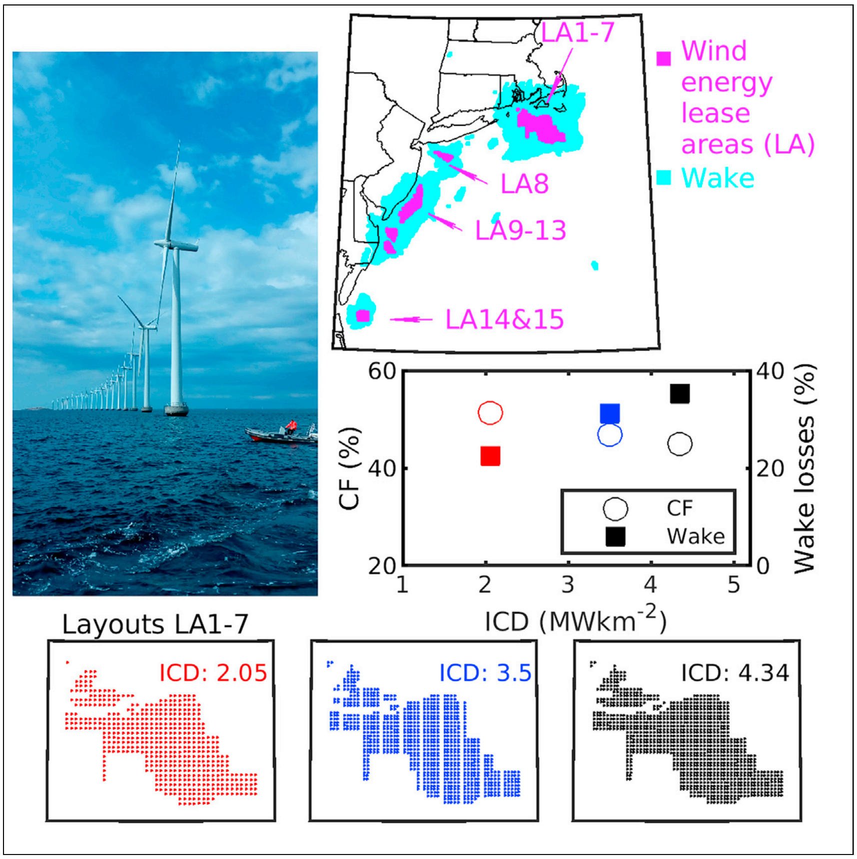

Many countries are planning development of very large offshore wind farms to aid decarbonization of the energy sector. High-resolution numerical simulations are performed to quantify power production (capacity factors [CFs]) and the spatial scale and effects of downstream wakes (areas of disturbed flow) from lease areas that are under development along the U.S. east coast. Descriptions of wake extent and power as a function of prevailing meteorology and wind-farm layout (installed capacity density [ICD]) are presented.

Sara C. Pryor, Rebecca J. Barthelmie, Tristan J. Shepherd

[redacted]

Highlights

Current U.S. east coast offshore wind lease areas can supply 3% of electricity

On average wakes extend over nearly 3-times footprint of the wind turbine arrays

Power and wakes are nonlinear functions of wind turbine density and meteorology

Guidance is provided for layouts of large offshore wind farms around the world

Pryor et al., Joule 5, 2663–2686
October 20, 2021 © 2021 Elsevier Inc.

[redacted]

Joule

Article

Wind power production from very large offshore wind farms

Sara C. Pryor,[1,3,*] Rebecca J. Barthelmie,[2] and Tristan J. Shepherd[1]

SUMMARY

We provide the first quantitative assessment of power production and wake generation from offshore wind energy lease areas along the U.S. east coast. Deploying 15-MW wind turbines, with spacing equal to the European average, yields electricity production of 116 TWh/year or 3% of current national supply. However, power production is reduced by one-third due to wakes caused by upwind wind turbines and wind farms. Under some flow conditions whole wind-farm wakes can extend up to 90 km downwind of the largest lease areas, and the frequency-weighted average area with a 5% velocity deficit is 2.6 times the footprint of the lease areas. Simulations including maritime corridors demonstrate reduction in the wake effects leading to power-efficiency gains and may offer contingent benefits. First-order scaling rules are developed that describe how "wake shadows" from large offshore wind farms scale with prevailing meteorology and wind turbine installed densities.

INTRODUCTION

The move to reduce energy-related greenhouse gas emissions is gathering international momentum fueled by both the urgent need to reduce anthropogenic forcing of climate[1–3] and rapid declines in the cost of renewable generation sources.[4] The government of the United Kingdom has committed to net zero greenhouse gas emissions by 2030. A critical part of that commitment is to deploy 40 GW of offshore wind, sufficient to power every home in the United Kingdom by 2030.[5] The European Commission's long-term strategy for decarbonization assumes the installation of 400 to 450 GW of offshore wind capacity within European waters by 2050.[6] In March 2021, the White House made a commitment to deploy 30 GW of offshore wind as part of a move to reduce U.S. greenhouse gas emissions by 50% from 2005 levels in 2030 and a carbon-pollution-free power sector by 2035 (see White House briefing at; [redacted] China has also committed to increasing the installed capacity of wind and solar power to over 1,200 GW by 2030 from 414 GW in 2019 (see press coverage at [redacted] This unprecedented and rapid expansion of offshore wind energy deployments affords opportunities to reduce anthropogenic climate forcing. It also raises challenges in terms of how to optimally locate wind turbines offshore at the scale required to achieve electricity-generation goals. This article provides timely and critical information to guide both U.S. and global offshore wind-energy deployments.

Estimated technically feasible potential electricity generation from U.S. offshore wind resources exceeds 7,000 Terra-Watt hours per year (TWh/year).[7] This surpasses current total national electricity generation of ~4,000 TWh/year.[8] As of May 2021, the U.S.

Context & scale

Massive upscaling of wind turbine deployments offshore is critical to achieving global and national goals to decarbonize the electricity supply. The excellent wind resource and proximity to large markets along the U.S. east coast mean it is the focus of America's first-phase offshore-wind projects. Thousands of physically larger and higher capacity wind turbines will be deployed over areas of unprecedented scale. The scale of these installations and those planned by other countries raises questions regarding potential reductions of electrical-power-production efficiency due to the operation of wind turbines in disturbed flow (wakes) from upwind wind turbines and wind farms. In this work, guidance is provided regarding the optimal layout of this new generation of wind farms to harness offshore wind resources in a manner that maximizes electricity production and minimizes the levelized cost of energy.

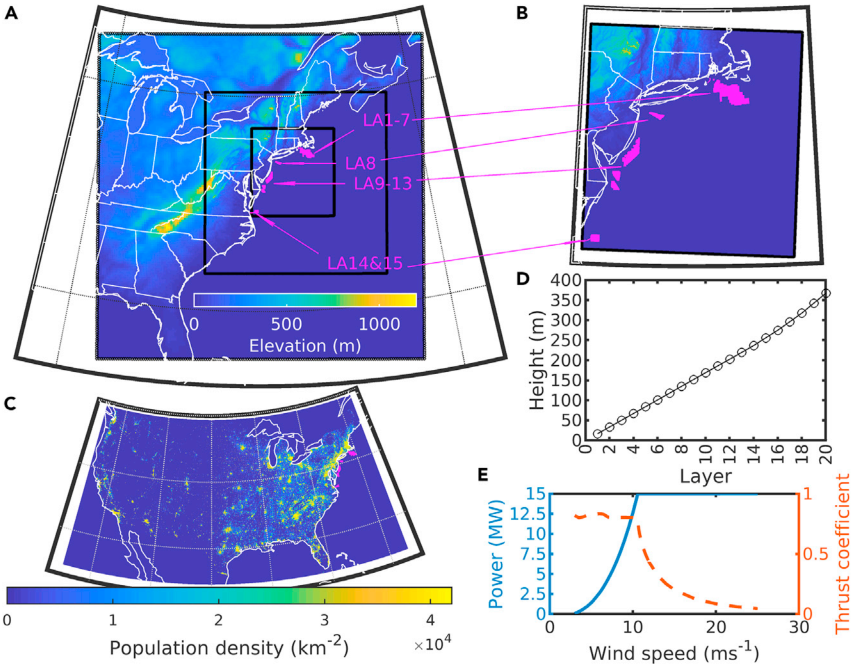

Figure 1. Overview of the simulations with the Weather Research and Forecasting (WRF) model and the locations of offshore wind-farm lease areas (LAs) along the U.S. east coast

(A) The outer WRF simulation domain (d01) has a grid resolution of 16.67 km. The second domain (d02) has a grid resolution of 5.56 km. Two inner domains (d03 and d04) comprise 340 × 361 grid cells and use a grid resolution of 1.85 km. The 15 offshore lease areas analyzed herein are shown by the magenta shading.

(B) The inner-most domain (d03 and d04) showing the lease area (LA) clusters.

(C) Proximity of the offshore lease areas to major demand centers as illustrated by the population density per km^2 according to the 2010 census (https://www.census.gov/data/tables/time-series/demo/popest/2010s-state-total.html) and the location of the 15 offshore lease areas (magenta).

(D) Mean height of the lowest 20 wind-speed levels computed for all water grid cells within d03.

(E) Wind turbine power and thrust coefficients as a function of wind speed (WS) for the IEA 15-MW reference turbine used in this analysis. This wind turbine has a HH of 150 m and rotor diameter of 240 m.[12] Power production begins at 4 ms^{-1} and ceases at WSs > 25 ms^{-1}, thus no power production or thrust coefficients are plotted for WSs outside of the range of 4–25 ms^{-1}.

had one 30-MW offshore wind farm operating at Block Island, Rhode Island, and two research turbines in Virginia.[9] However, the current total U.S. offshore wind pipeline (to 2030) is over 26 GW, much of which is focused on 16 lease areas (LAs) along the east coast[10] (Figures 1A and 1B). Realizing this pipeline would increase current U.S. wind turbine installed capacity (IC) by over 20% and almost double total global offshore installed capacity, which was 28 GW at the end of 2019.[11]

Expansion of the U.S. offshore wind industry represents a substantial financial investment. Data from Germany indicate the total installed project cost for offshore wind turbines of US$ 1,910 per kilo-Watt (kW) during 2019.[13] Projections for fixed bottom offshore wind turbines in the U.S. made in 2019 indicate total capital expenditure of US$ 4,077 per kW.[14] Using these cost estimates, installation of 26–29 GW in the 16 LAs off the U.S. east coast, equates to a direct investment of ~US$ 50 to 120 billion.

The global trend toward increased deployment of wind turbines offshore is associated with declining levelized cost of energy (LCoE), and offshore projects in the mature markets of Germany and the Netherlands are now subsidy free.[13] The

[1]Department of Earth and Atmospheric Sciences, Cornell University, Ithaca, NY 14853, USA

[2]Sibley School of Mechanical and Aerospace Engineering, Cornell University, Ithaca, NY 14853, USA

[3]Lead contact

*Correspondence [redacted]

transition to offshore deployments is driven by multiple factors. First, wind speeds are generally higher and more persistent than over land surfaces, leading to higher efficiency of electrical-power production.[11] The variation of electrical-power production from wind turbines with wind speed is described using a power curve (Figure 1E). Power production increases as wind speeds increase from cut-in when power production begins (commonly about 4 ms^{-1}) to a threshold at which the power production reaches the rated power and no longer continues to increase with increasing wind speed. This rated power thus describes the amount of electrical power in watts (i.e., joules per second) a wind turbine generates if it is operating at optimal wind speeds. Due to factors such as lower surface roughness and the absence of orographic barriers, wind turbines deployed offshore generally operate more frequently at rated power than those located onshore. Second, many major urban areas are located in coastal areas, providing nearby load centers for the electricity generated by offshore wind farms. For example, the Boston-Washington corridor, encompassing New York City, has a population over 50 million and is located close to the U.S. east coast offshore LAs (Figure 1C).

A major source of uncertainty in designing offshore wind turbine arrays (wind farms) and optimal spacing between wind farms derives from power-production losses[15,16] and enhanced fatigue loading[17] caused by operation of a wind turbine or wind farm in the wake of an upstream wind turbine or wind farm.[18] Wakes are flow regions behind wind turbines and wind farms that are characterized by lower wind speeds and higher turbulence levels and are caused by the extraction of momentum by wind turbines. The magnitude of these wakes and the downstream distance necessary for them to be eroded by mixing with surrounding high-momentum air is primarily determined by: (1) wind speed across the wind turbine rotor. This determines the efficiency of momentum extraction. The wind turbine thrust coefficient describes the magnitude of the wind-speed reduction and amount of turbulence introduced by the rotor as a nonlinear function of the incident wind speed (Figure 1E).[15] (2) Turbulence from mechanical and thermal sources. The turbulence intensity and the depth of the planetary boundary layer dictate the rate at which kinetic energy can be transferred down the velocity gradient into the wind turbine wake. For a given wind turbine or wind farm, as shown herein, these three atmospheric variables; wind speed, turbulence intensity, and boundary layer depth are largely responsible for dictating the downwind distance necessary for the flow to return to its undisturbed condition, i.e., for the wake to recover.[15,16,19] The rate at which kinetic energy can be transferred in the atmosphere limits the amount of energy that can be extracted by wind turbines per unit of surface area.[20–22] Low transfer rates can reduce power production from wind turbines in the interior of large offshore wind farms to approximately 60% of what would be achievable if all wind turbines experienced undisturbed air flow.[15,16] Low turbulence and planetary boundary layer depths offshore also mean that cumulative wind-farm wakes persist over longer downwind distances[23,24] and that wake-induced power loss within wind farms are also larger than in onshore wind farms.[15,16] (3) Wind turbine spacing: closer spacing means more wind turbines operate in the wake of upstream turbines and thus experience lower wind speeds and generate less electrical power. For example, the Horns Rev I offshore wind farm in Denmark has an IC of 166 MW, a turbine spacing of 7 × 7 rotor diameters (D) and mean reduction in power production due to wakes from upstream turbines impinging on downstream wind turbines (wake losses) of 12.4%.[25] Conversely, Lillgrund, in the coastal waters of Sweden, which has a similar IC (of 110 MW) but uses a smaller distance between wind turbines (a spacing of 3.3 to 4.3 D), exhibits wake losses of 23%.[25] (4) Wind direction: wind direction determines the likelihood that wind turbine wakes within an array interact with each other and whether the wake from one wind turbine array will be advected over another.[23,26]

The number of global offshore wind farms, the size and rated capacity of the wind turbines, and the total IC within individual arrays are increasing. For example, the mean IC of European offshore wind farms doubled from 321 to 621 MW between 2010 and 2019.[27] The largest operating offshore wind array is Hornsea Project One. It has a total IC of 1.2 GW over a deployment area of 630 km^2.[28] Despite the growth in installed capacities, the most recently built European offshore wind farms continued to employ wind turbine spacing of 4 to 11 rotor diameters (D) with a mean of 7.7D.[29] Offshore wind farms operating in Europe have installed capacity densities (ICDs), i.e., the rated power of the installed wind turbines per square kilometer of ground area) of 2.5 to 12 MWkm^{-2}.[30] An additional analysis of data from offshore wind farms in Europe indicates mean ICDs of 3 to 7.2 MWkm^{-2}, depending on the definition of wind farm areal extent.[31] There has also been a pronounced trend toward deployment of physically larger and higher-rated power wind turbines.[32] These industry trends are causing an increased probability of large wake losses within individual wind farms and an increased probability of wake interactions between offshore wind-turbine arrays.[33,34] Further, a recent meta-analysis identified wake-induced power losses as the primary source of uncertainty in preconstruction estimates of annual energy production from wind turbine arrays and a major contributor to excess project financing costs.[35] Improved understanding of wind turbine and wind-farm wakes is thus essential to ensuring the planned global investments in offshore wind achieve the electricity-generation goals and do so at the lowest possible cost.

The objective of this work is to characterize power production, wind-farm wake intensity and extent, and wake-induced power losses from planned very large offshore wind farms. This work is focused on much larger offshore wind turbine arrays than are currently operational but have a scale equal to those that are anticipated to be developed in the U.S., Europe, and China. It thus extends the literature that has previously focused primarily on smaller wind turbine arrays or has considered the limit case of nearly infinite wind farms. This work also includes an analysis of the sensitivity of power production and wake effects to both wind-farm ICD and meteorology for a wide range of atmospheric conditions that prevail offshore. Two methodological innovations are presented. A flow-scenario method is introduced to efficiently develop robust assessments of power production, wake extent and intensity, and wake-induced power losses. The concept of the normalized wake extent is also introduced and statistical models of this property as a function of prevailing meteorology are developed. The numerical simulations are performed for the existing offshore LAs along the U.S. east coast but the study findings have relevance to the global offshore wind-energy industry.

Offshore wind LAs along the U.S. east coast

LAs for possible offshore wind development in the U.S. are auctioned and managed by the Bureau of Ocean Energy Management (BOEM). The 15 offshore LAs considered here lie along the coasts of the Northeast and Atlantic U.S. states (Figures 1A and 1B[10]). Each has a unique alpha-numeric identifier; OCS-A-NNNN, where NNNN is unique to the LAs. LAs 1–7 are treated as a LA cluster herein. All seven lie within a coherent area along the coast of Massachusetts and Rhode Island and collectively cover 3,675 km^2. These include OCS-A 0487, 0500, 0501, 0520, 0521, 0522 (listed west to east) that are adjacent to one another, while OCS-A 0486 is separated from 0487 by a channel that is 2.4 km wide. LA 8 (0512) is located off the coast of New York state and covers an area of 321 km^2. LAs 9–13 cover a total area of 2,105 km^2. Two of these LAs are adjacent and are offshore from New Jersey (OCS-A 0499 and 0498). They are 23 km north of two LAs east of Delaware (OCS-A 0482 and 0519), that are 11 km north and east of the sole Maryland LA (OCS-A 0490). These five LAs are not all adjacent but are treated as a cluster here because, as shown herein, under certain flow conditions the wake from these LAs exhibit substantial overlap. LAs 14 and 15 (OCS-A 0483 and 0497) are adjacent, cover an area of 465 km^2 and are located off the coast of Virginia. The final LA, OCS-A 0508, lies further south off the coast of North Carolina. It is not included in the innermost simulation domain and is thus excluded from consideration in this analysis.

The total extent of the LAs considered here is 6,566 km^2. This, and the spatial scale of the individual and contiguous offshore LAs along the U.S. east coast, greatly exceeds that of current European offshore wind farms. However, they are representative of the scale of future wind turbine deployments needed to meet the expressed goals of the United Kingdom, the European Union, the United States of America, and China. Quantifying power losses due to wakes as a function of atmospheric conditions (e.g., wind speed, planetary boundary layer height, and ambient turbulent kinetic energy) and ICD will inform wind turbine array layouts, and aid power-production forecasting and grid-integration planning in both the U.S. and beyond. The close proximity of these current LAs (Figures 1A and 1B) and prospective future LA offerings along the U.S. east coast[36] and the planned expansion of wind turbine deployments in the North Sea[6] further emphasize the need to quantify possible array-array interactions, particularly as adjacent LAs are owned and operated by different companies or consortia.

Simulations with the Weather Research and Forecasting (WRF) model are performed using nested domains resolved with high horizontal and vertical resolution (Figures 1A, 1B, and 1D). The modified Fitch wind-farm parameterization is used to quantify power production and wakes.[37,38] Wind-farm parameterizations such as Fitch seek to treat the bulk aerodynamic effects caused by wind turbines within and downwind of the grid cell(s) in which they are located. An estimate of the power produced by the wind turbine(s) in each grid cell and model time step is computed from the wind turbine power curve (Figure 1E) and the grid-cell-averaged incident wind-speed profile across the rotor plane. The wind turbine(s) within a given grid cell impose a drag force across the rotor plane that is determined by the wind turbine thrust coefficient (Figure 1E) and the incident wind-speed profile. This drag force removes kinetic energy from the flow resulting in a modified wind-speed profile that is advected to adjacent grid cells. Turbulent kinetic energy is added to the flow at a rate proportional to the fraction of kinetic energy extracted by the wind turbine and not converted into electrical power. It too is advected into adjacent grid cells. The wind-farm parameterization thus requires information regarding wind turbine physical dimensions, along with power and thrust coefficients that are often held confidential by wind turbine manufacturers. Therefore, the International Energy Agency (IEA) reference turbine[12] is employed, having a similar hub height (HH) and rotor diameter (D) to the G.E. Haliade-X 13-MW wind turbine (HH $\sim$ 140 m, D $\sim$ 220 m) that has been selected for LA 1.

The methodology used to efficiently generate a robust assessment of likely power production and wake losses from the U.S. east coast LAs is derived from earlier work on wind-resource assessment.[39] We identify dominant modes of relevant atmospheric flow conditions and then perform simulations for real 5-day periods that reflect those flow scenarios (Figure 2). The results from these simulations are weighted by the frequency with which each flow scenario occurs to derive climatologically representative power-production and wake statistics. The flow scenarios are abbreviated using the following nomenclature: WDWS (where WD is the wind direction and WS is the wind speed e.g., NE4-10 for northeasterly flow in the

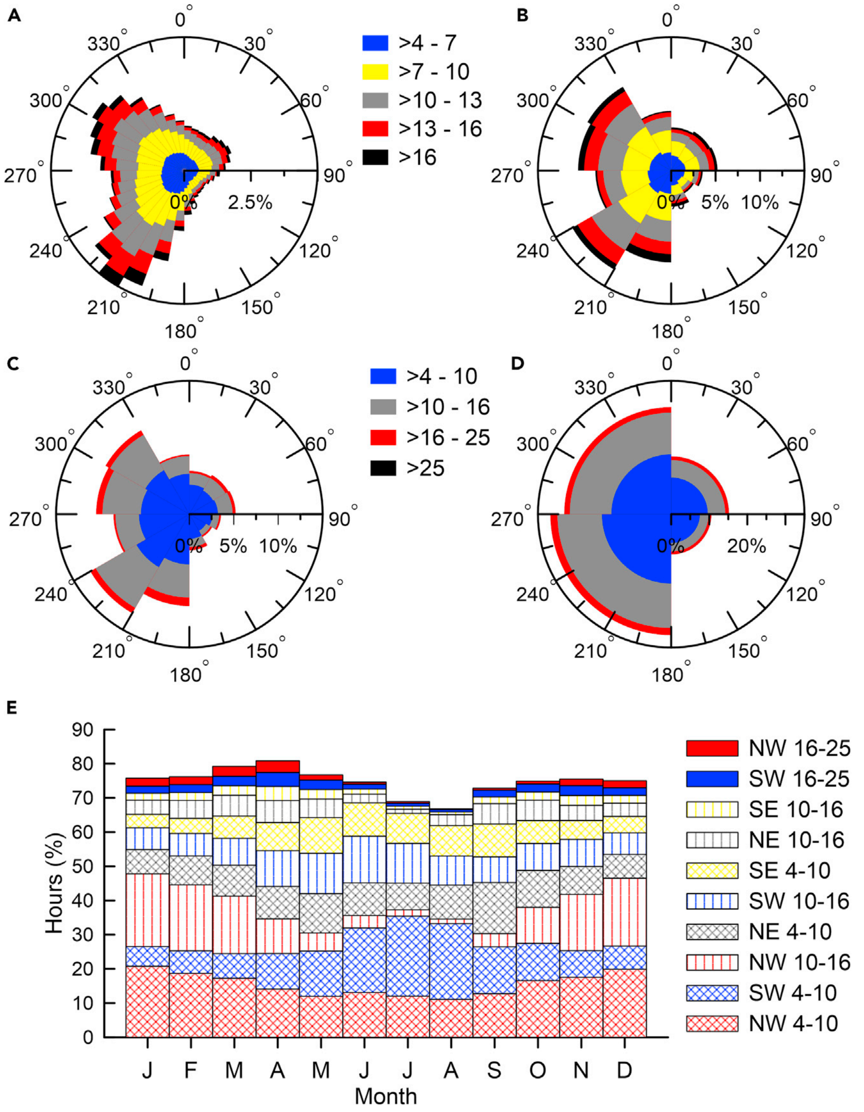

Figure 2. Overview of hourly wind speeds and directions at 100 m height in lease area 8 and the aggregation approach used to define the flow scenarios and characterize their frequency and seasonality

(A) Wind rose of all ERA5 hourly observations from 1979–2018 for the grid cell containing lease area 8 (Figures 1A and 1B) wherein the wind speeds (WSs) are discretized into 3 ms^{-1} classes for all values above 4 ms^{-1}, and wind directions (WDs) are discretized into 10° classes.

(B) As in (A) but using 30° wind direction sectors.

(C) As in (A) but for WSs in 6 ms^{-1} classes.

(D) As in (A) but using 90° wind direction sectors.

In each (A–D), the radial axis denotes the percentage of hours with wind speeds between 4 and 25 ms^{-1} that fall into the specified flow class. The ten most frequently observed combinations of wind direction and speed (denoted by WDWS) are (in rank order); SW4-10, SW10-16, NW4-10, NW4-10, NE4-10, SE4-10, NE10-16, SE10-16, SW16-25 and NW16-25.

(E) Frequency of the flow scenarios by calendar month as a percentage of hours in each month. The flow scenarios are ordered by frequency with the most frequent at the bottom. Red shading denotes northwesterly (NW) flow, blue for southwesterly (SW), black for northeasterly (NE), and yellow for southeasterly (SE) flow. Crosshatching indicates wind speeds (WS) of 4 to 10 ms^{-1}, vertical lines denote WS between 10 and 16 ms^{-1}, and the solid shading indicates WS between 16 and 25 ms^{-1}.

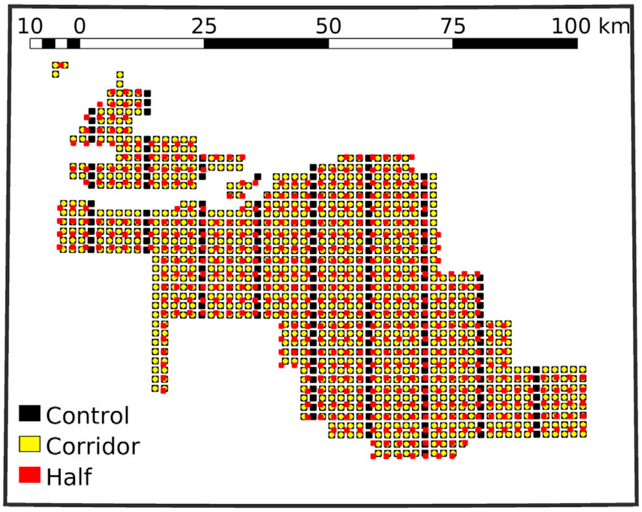

Figure 3. Illustration of the three wind-turbine deployment layouts for the lease areas 1–7 cluster (see location in Figure 1)

The black squares denote the placement of wind turbines within this cluster of lease areas in the control deployment layout with wind turbine separation of 1.85 km (for a mean installed capacity density of 4.34 $\mathrm{MWkm^{-2}}$). The yellow circles denote placement of wind turbines in this cluster of lease areas in the maritime-corridor deployment layout (i.e., where the sixth north-south row of wind turbines from the control are removed). The red squares denote placement of wind turbines in this cluster of lease areas in the half-density deployment layout.

wind-speed class 4–10 $\mathrm{ms^{-1}}$). The simulation periods are referred to here use the date; YYYY-MM-DD (i.e., year-month-day) of the first day of each 5-day period.

Simulations are performed for three different wind turbine layouts and ICD (Figure 3): (1) a control layout using the average wind turbine spacing from Europe (i.e., 7.7 wind- urbine rotor diameters), which means that the distance between each wind turbine is 1.85 km. This spacing has been selected for LAs 1 through 7. It yields a total IC of 28.8 GW from 1922 wind turbines of 15 MW each. For this wind turbine layout the mean ICD across the four clusters of LAs is 4.34 $\mathrm{MWkm^{-2}}$. (2) A maritime-corridor layout where the sixth north-south "column" of wind turbines in each LA is removed. This reduces the total IC to 24.1 GW. (3) A half-density layout for a total installed of 14.5 GW. The ICD for this layout (~2.1 $\mathrm{MWkm^{-2}}$) is at the lower end of current offshore wind farms in Europe.

The distribution of wind turbines between the LA clusters are as follows. In the control simulations there are 1,073 wind turbines deployed in LAs 1 through 7, 89 in LA 8, 624 in LAs 9 through 13, and 136 in LAs 14 and 15. When the maritime corridors are introduced, the total number of wind turbines in each LA cluster drops to 900, 74, 521, and 109, respectively. In the half-density layout the wind turbines are separated by ~2.8 km, and the equivalent wind turbine numbers deployed in each LA cluster are, respectively, 532, 47, 318, and 71.

Output from each of the eleven, 5-day simulations of the control layout is weighted using the relative frequency of the flow conditions it represents to derive robust estimates of expected power production and a wake climatology from the U.S. east coast LAs. The same analysis is performed for simulations of the other wind-farm layouts. Model output for the control and half-density wind-farm layouts are also used to develop first-order scaling rules that describe how the area influenced by wakes from an offshore wind farm depends on the prevailing atmospheric conditions and the density of wind turbines within the wind farm.

RESULTS

Estimated power production from the U.S. offshore LAs

After applying frequency weighting to output from the 5-day simulations of each of the 11 flow scenarios, the expected electric-power production for the control layout is 116 TWh/year or 3% of current national supply. Electric-power production from wind turbines is summarized using capacity factors (CFs) computed as the ratio of the amount of power produced normalized by the potential power produced if all wind turbines run at their rated capacity (in this case, 15 MW). The mean CF for the control layout, where the wind turbines are spaced at the mean value from operating offshore wind farms in Europe, is 45.8% (Table 1). Power losses due to transmission, curtailment for grid operation, and operations and maintenance actions for onshore wind farms decrease CFs in the U.S. by an average of 4 percentage points.[40] Assuming that this estimate is also appropriate for offshore wind turbine arrays, the resulting estimated net-CF for these U.S. east coast offshore LAs is ~42%. This is comparable with, or better than, values reported for European (38% during 2019[41] and 40.8% cited in a meta-analysis[31]) and global (40% to 42%[11]) offshore wind farms. Thus, this modeling suggests that if the U.S. LAs are developed using wind turbines similar to the IEA 15-MW reference wind turbine laid out at a spacing equal to the mean in European offshore wind farms, they would operate with the same, or higher, CFs than those in smaller offshore wind farms in Europe that have been shown to be highly viable economically.

There is substantial variability in power production across the flow scenarios with, as expected, higher freestream wind speeds being associated with higher CFs (Figure 4A; Table 1). The higher CFs for the northern LAs (LA cluster 1–7 and LAs 8; Figures 4A and 5A) are due to: (1) higher wind speeds and thus better wind resources (Figure 5B) and (2) smaller wake losses in the smallest contiguous LA of wind turbine deployments (lease area 8, LA8) (Figures 4B and 5A). The south-north gradient of increasing wind-resource magnitude implied in the 11 simulations of the individual flow scenarios is consistent with wind-resource estimations from long-term reanalyses,[10] mesoscale simulations, and satellite-derived wind climates.[42] The most northern and largest cluster of LAs (1 through 7; see Figure 1B) exhibit a frequency-weighted mean CF of 46%, while in LA 8 it is 56%, in lease areas 9–13 it is 45% and lease areas 14 and 15 have a mean CF of 40% (Table 1; Figures 4B and 5).

Each of the LA clusters exhibits different CFs for the diverse flow scenarios due in part to variations in wind direction, and hence the over-water fetch and the resulting levels of turbulent kinetic energy (TKE) and wind speeds at the wind turbine HH (Figure 4C). For example, LAs 14 and 15 exhibit the highest mean CFs for the northeasterly flow scenarios (NE10-16 and NE4-10, represented by simulation periods that commence on 1985-11-28 and 2012-11-17) and lowest mean CFs for flow directions that are from land (NW4-10 and SW4-10, represented by simulation periods that commence on 1988-07-04 and 1998-06-04) (Figure 4B).

Two sets of sensitivity simulations for different wind turbine layouts are performed for a subset of atmospheric flow conditions. Implementation of maritime corridors reduces overall power production due to the decrease in the number of wind turbines (from 1,922 to 1,604) but increases mean CFs by 2 percentage points due to the reduction in wake losses (Figure 4A; Table 1). Reducing the wind turbine

Table 1. Summary of the flow scenarios and simulation results

		ERA5: lease area 8 centroid				Control					Corridor		Half	
Flow scenario	Start date of 5 day	% of obs.	100-m WS class (ms^{-1})	100-m wind direction class (°)	# of hours out of 120 in class	Mean CF (%)	Mean wake loss (%)	Area of d04 with $<v_d>$ of 2% (%)	Area of d04 with $<v_d>$ of 5% (%)	Area of d04 with $<v_d>$ of 10% (%)	Mean CF (%)	Mean wake loss (%)	Mean CF (%)	Mean wake loss (%)
NW4-10	1979-10-26	7.85	4–10	270–360	66	26.7	34.4	4.1	2.3	1.3	28.3	30.5	32.1	21.2
SW16-25	1981-04-04	1.6	16–25	180–270	43	76.0	13.5	7.7	3.7	1.7	–	–	–	–
SE4-10	1981-08-29	7.5	4–10	90–180	78	22.9	65.5	8.8	5.6	3.8	–	–	–	–
NE10-16	1985-11-28	4.6	10–16	0–90	64	73.6	17.5	7.6	3.3	1.6	–	–	–	–
SW10-16	1986-03-26	9.1	10–16	180–270	69	53.0	31.1	12.3	6.2	3.6	56.2	27.0	63.4	17.4
SW4-10	1988-07-04	12.5	4–10	180–270	84	9.0	64.7	14.1	4.7	2.7	10.1	60.3	13.6	47.0
NW4-10	1998-06-04	7.85	4–10	270–360	78	42.8	34.6	5.6	3.4	2.2	–	–	–	–
NW16-25	2000-01-17	1.4	16–25	270–360	32	60.7	6.8	3.6	1.6	0.2	–	–	–	–
NW10-16	2007-02-05	11	10–16	270–360	84	88.7	4.2	2.8	1.4	0.3	89.6	3.3	91.0	1.7
SE10-16	2011-05-15	2.3	10–16	90–180	37	63.3	20.7	7.7	5.0	2.9	–	–	–	–
NE4-10	2012-11-17	9.6	4–10	0–90	90	49.1	34.4	10.3	3.9	2.0	52.0	30.5	59.9	20.1
Frequency-weighted means. Two values are given for the control.						45.8[a] 45[b]	35.3[a] 34.7[b]	–	–	–	46.9	31.3	51.4	22.5

Columns on the left define the flow scenarios and the 11 5-day periods used to represent each scenario (by start date). Subsequent columns show the flow-scenario frequency based on ERA5 WS and wind direction at 100 m from the grid cell containing lease area 8 (LA8), along with the number of hours in the 5-day period that fall within the flow class. Results of the WRF simulations are shown for three different wind-turbine layouts: control in which the lease areas are fully occupied by wind turbines deployed with a 1.85 km spacing. Corridor where every sixth north-south row of wind turbines is omitted. Half (for half-installed capacity density) where the wind-turbine spacing is increased to 2.6 km (see details in Figure 3). The mean CF shown is derived from 10-min power production output from wind turbines in all lease areas. Mean wake losses are computed using the power production from the wind-farm parameterization and the maximum power possible if all wind turbines experienced the freestream WS. For the control layout the percentage of the grid cells in the innermost domain that exhibits a mean velocity deficit (v_d) of 2, 5, and 10% is also shown. Slightly over 1.5% of simulation domain d04 grid cells contain wind turbines in the control simulations.

[a] Frequency weighting across all flow scenarios.

[b] Frequency weighting of only flow scenarios also used in Corridor and half simulations.

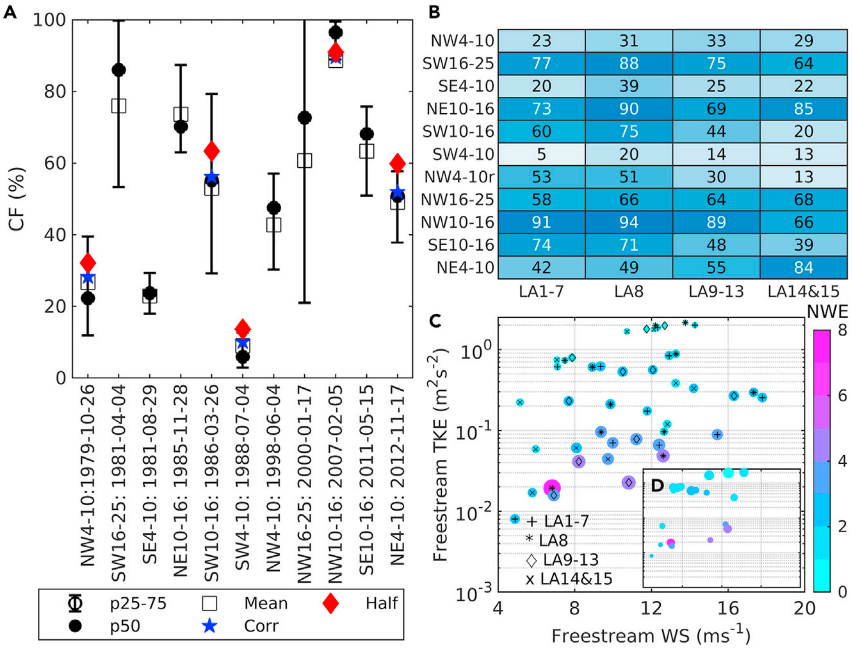

	LA1-7	LA8	LA9-13	LA14&15
NW4-10	23	31	33	29
SW16-25	77	88	75	64
SE4-10	20	39	25	22
NE10-16	73	90	69	85
SW10-16	60	75	44	20
SW4-10	5	20	14	13
NW4-10r	53	51	30	13
NW16-25	58	66	64	68
NW10-16	91	94	89	66
SE10-16	74	71	48	39
NE4-10	42	49	55	84

Figure 4. Capacity factors (CFs, in %) and wake extents for each of the 5-day periods that represent the 11 flow scenarios

(A) Mean, median (p50), and interquartile range (p25–75) of 10-min systemwide CFs (i.e., all lease areas) for each flow scenario in the control simulations (black). Also shown are mean capacity factors for simulations of wind turbine layouts including maritime corridors (blue stars) and half wind turbine density (red diamonds). Labels on the bottom axis indicate the flow scenario and start date of each 5-day simulation period.

(B) A heat map of mean capacity factors (CFs, in %) in each lease-area (LA) cluster for each flow scenario from the control simulations. Note: two cases are simulated for the most common flow scenario; northwesterly flow with WSs from 4 to 10 ms^{-1} (NW4-10), one in fall and one in summer (denoted by the r). The first lease area cluster (LA1–7) is located south of Massachusetts. Lease area 8 (LA8) is located off the coast of New York state. Lease areas 9–13 (LA9-13) are located offshore of New Jersey, Delaware, and Maryland. Lease areas 14 and 15 (LA14&15) are located off the coast of Virginia (Figures 1A and 1B).

(C) Normalized wake extent (NWE) calculated as the area covered by a mean velocity deficits of over 5% ($v_d \leq -0.05$) divided by the spatial extent of the lease-area cluster that generates the wake using Equation 6) for the control simulations plotted as a function of the mean freestream wind speed (WS) and turbulent kinetic energy (TKE) at 150 m in height over each lease-area cluster. There are 11 simulations and 4 lease-area clusters, thus 44 data points are plotted. The symbol size and color denote the normalized wake extent (NWE), and the marker in each NWE estimate denotes the lease-area cluster for which it is derived.

(D) (Inset to C) Difference in NWE (ΔNWE, Equation 7) plotted as a function of the mean freestream WS and TKE at 150 m over each lease-area cluster. Symbol size scales with the magnitude of ΔNWE between the control layout and half-density simulations (range 0.15–0.95), while the color denotes normalized wake extent (NWE) in the control simulations.

installed density to half of that used in the control simulations (968 wind turbines) further reduces power production but again increases mean CFs (Figure 4A; Table 1). Frequency-weighted mean CFs based on this subset of five flow scenarios increases from 45% in the control, to 46.9% in the corridor layout, and to 51.4% in the half-density layout (Table 1). This demonstrates the highly nonlinear dependence of power production and wake losses on atmospheric conditions and wind turbine spacing. Simulations such as those presented herein, which consider different wind turbine layouts, have high value in guiding development of large offshore wind farms in spatially limited LAs, particularly when they address other stakeholder interests (e.g., corridors to enable fishing and shipping) and can contribute to life-cycle financial analyses.[44]

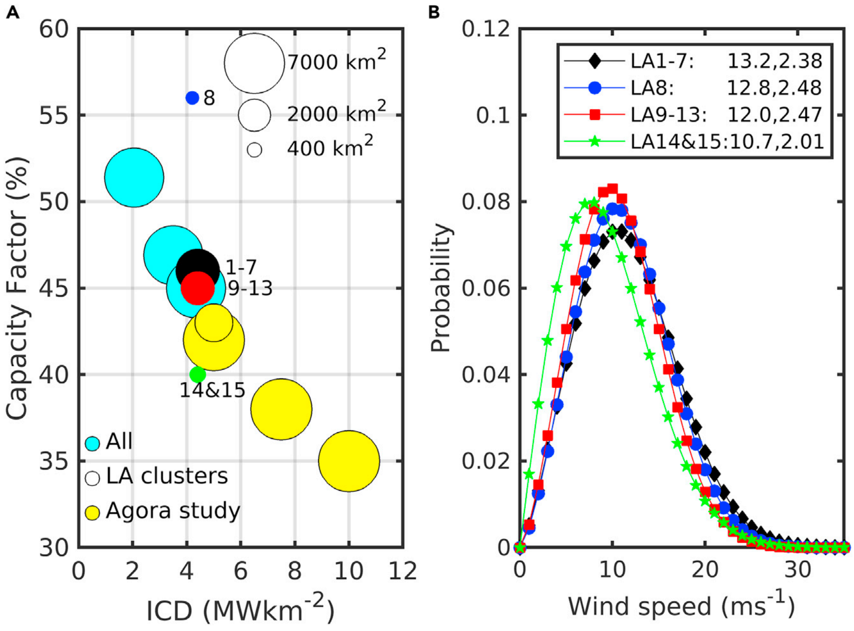

Figure 5. Capacity factors and wind speed probability distributions for the U.S. east coast lease area clusters

(A) Mean capacity factor (CFs in %) versus installed capacity density (ICD in MWkm^{-2}) for varying wind turbine deployment layouts and across the four lease-area (LA) clusters. The symbol diameter in (A) scales with the area over which the wind turbines are deployed (see legend, upper right). Results from this study are shown accumulated over all four lease-area clusters (cyan) for the three wind-turbine deployments—control, maritime corridors, and half-installed capacity density—(ICD), and for each the four lease-area (LA) clusters (colors as in B) from the control deployment (ICD ~ 4.34 MWkm^{-2}) with the numbers indicating the lease-area clusters (LAs 1–7, 8, 9–13, and 14 and 15) (see Figures 1A and 1B). Also shown are results of a study for projected developments in the German Bight area of the North Sea from the Agora study.[6] Both analyses are based on simulations with the Weather Research and Forecasting (WRF) model, but use different wind-farm parameterizations; Fitch[37,38] is shown here and the Explicit Wake Parameterization (EWP)[43] in the Agora study. Results from the Agora study are shown for 12-MW wind turbines deployed at an installed capacity density (ICD) of 5 MWkm^{-2} over an area of 2,767 km^2, with an installed capacity (IC) of 13.8 GW, and in two large arrays covering areas of 2,767 km^2 and 4,473 km^2 (total IC of 36.2 GW), and for those two deployment areas at ICD of 7.5 MWkm^{-2} (total IC of 54.3 GW) and of 10 MWkm^{-2} (total IC of 72.4 GW).

(B) Probability distributions from a two-parameter Weibull fit to modeled freestream wind speeds (WSs) at a height of 153 m a.s.l. in the center of each lease-area (LA) cluster. The numbers in the legend in (B) indicate the Weibull A and Weibull k parameters derived using maximum likelihood estimation and Equation 3.

Estimated wake intensity and spatial extent

Despite the relatively high CFs that measure the actual energy output relative to the maximum possible, these model simulations also indicate substantial loss of potential power production due to the impingement of wakes on downstream wind turbines within individual LAs and between LAs (Figure 6). Individual LAs, and not only those that are immediately adjacent, are projected to be frequently operating in the "wind shadow" of upstream wind farms (Figure 6). This not only reduces power production but will be associated with increased mechanical loading on the wind turbines.

Frequency-weighted wake-induced power losses averaged over all LAs are 35.3% (Table 1). Thus, over a third of potential electrical-power production that could be achieved if all wind turbines operated in freestream (undisturbed) flow is lost due

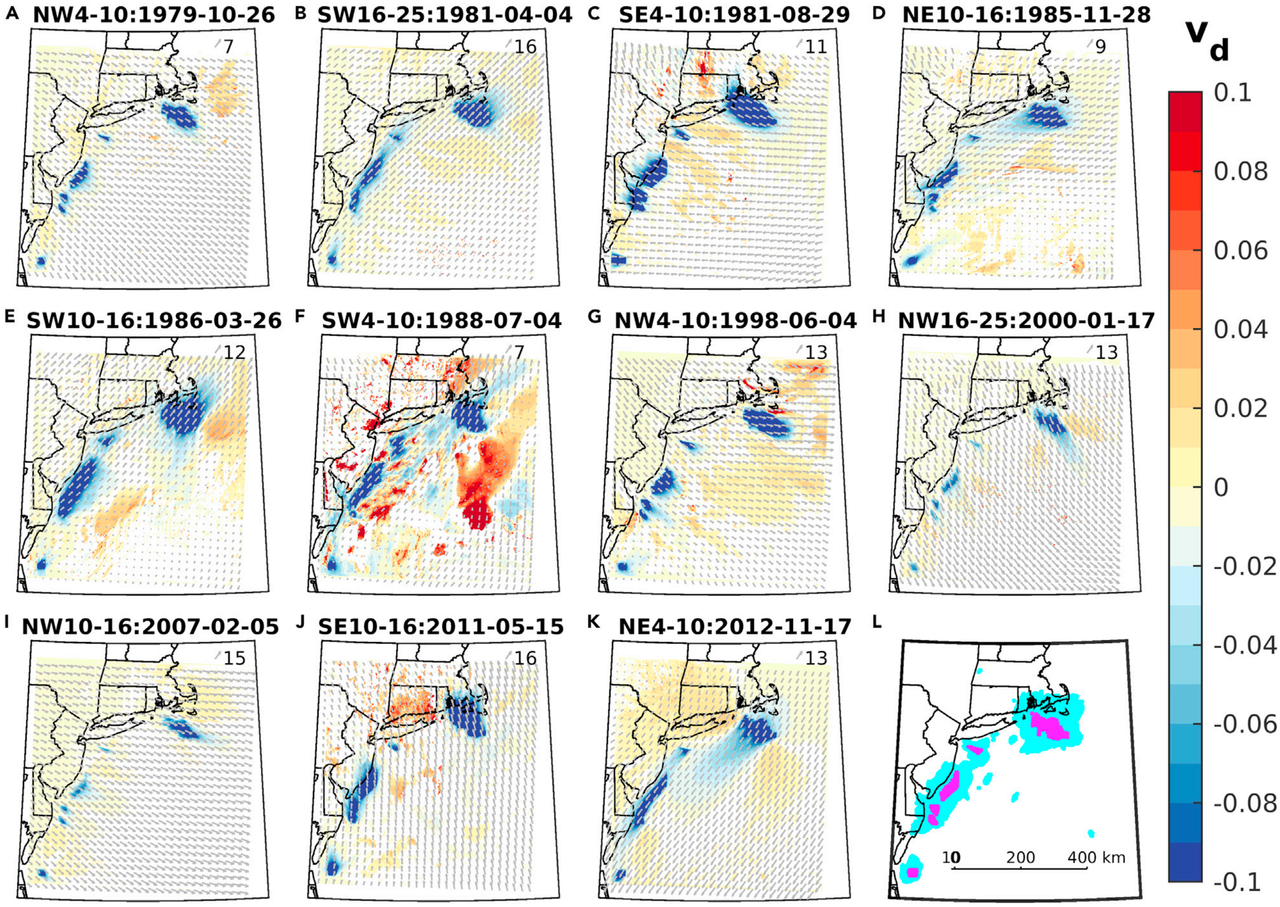

Figure 6. Mean velocity deficit (v_d) in each grid cell for each of the 5-day flow-scenario simulations (Table 1)

(A–K) The title of each panel denotes the flow scenario (the first two letters denote the wind direction and the digits indicate the WS class) and first day of each 5-day simulation period (date is written as year-month-day). The mean velocity deficit is the mean normalized difference in WS in each grid cell at each time step (i) in output from simulation domain d04 (operating wind turbines) to output from simulation domain d03 (no wind turbines) (see Equation 4). The overlying quivers are the mean WS and direction computed using output from the simulation domain d03 that describes the freestream conditions. For legibility, the quivers are plotted at the 12th grid cell in both the latitude and longitude positions and are scaled to prevent overlap. The maximum length of each quiver in each panel is set to the maximum mean WS plot for each case (shown in the upper right of the panel and expressed in ms^{-1}).

(L) Composite of all grid cells that have a mean velocity deficit of 5% or more ($v_d \leq -0.05$) in one or more of the flow cases (cyan) and the location of grid cells containing wind turbines (magenta).

to their operation within wakes from upstream wind turbines and wind farms. This value greatly exceeds wake losses from current European offshore wind farms[25] in part because of the very large extent of the wind-farm clusters and unprecedented number of wind turbines deployed.

Velocity deficits (v_d) are used here as a metric of wake intensity and extent. They represent the reduction in wind speed relative to what would be observed if no upstream wind turbines are present. These velocity deficits are calculated using wind speeds at the wind turbine HH from simulation domain d04 output with the action of wind turbines included (WS_{WT}) and output from simulation domain d03 where no wind turbines are included (WS_{NoWT}) (see methods). The concept of the normalized wake extent (NWE) is introduced to describe the areal extent of disturbed flow caused by a given wind farm. It is the ratio of the spatial extent of the wind shadow generated by a wind farm to the area of the wind farm. The NWE is naturally a function of the threshold of velocity deficit used to define the wake. The area covered by mean velocity deficits of 2% (i.e., $v_d \leq -0.02$, Equation 4) for the 11 flow scenarios with the control layout ranges from 2.8% to 14.1% of the innermost model domain where wind turbines are operating (d04), while the area covered by wind turbines is 1.5% (Table 1). Thus, the mean NWE using this velocity deficit threshold varies depending on the prevailing atmospheric conditions but is between two times and nearly ten times the spatial extent of the wind farms. Similar mean NWEs computed for the different flow scenarios using a velocity deficit (v_d) of 5% range from one to four, with a weighted mean of 2.6. Using a velocity deficit (v_d) of 10% to define the area covered by a wake, the mean NWE in each 5-day simulation ranges from 0.15 to nearly three (Table 1). These values indicate that, consistent with expectations, wind turbine deployments within these LAs will generate substantial downstream "wind shadows" (Figure 6). As discussed further below, large, NWEs are associated with simulations of flow conditions characterized by moderate wind speeds, low ambient turbulence, and low planetary boundary layer depths.

The NWE is substantially smaller in the half-density simulations for all LA clusters and all values of freestream wind speed, planetary boundary layer height, and TKE (Figure 7). The mean difference in normalized spatial wake extents in the control and half-density simulations (ΔNWE, computed using Equation 7) is 0.48. Thus, the area covered by mean velocity deficit of at least 5% reduces to half the value from the control simulations when a half-density wind turbine layout is simulated. Thus, on average, there is a systemwide benefit from minimizing wind shadows from upstream LAs by locating wind turbines with greater spacing. However, the range of ΔNWE extends from 0.12 to 0.96, indicating that under some atmospheric flow conditions the NWE is only modestly influenced by the density of wind turbine deployments in the LAs. The difference in NWE in the half-density simulations relative to the control is maximized for periods with high ambient turbulence (Figure 4D). Thus, the decrease in wake extent due to the reduction in ICD is disproportionately weighted toward periods with relatively small, NWEs in the control simulations. The BOEM intends to auction additional LAs close to these existing LAs. While adoption of lower ICD will reduce revenues to individual LA operators, it may have benefits in terms of reducing systemwide power losses and wind turbine fatigue loading due to wakes within wind farms and between wind farms.

An alternative metric of the wind-farm wake extent is the maximum distance downwind from LA clusters aligned with the mean wind direction to which a mean velocity deficit of at least 5% ($v_d \leq -0.05$) extends (Figure 6L). For the control simulations, the minimum downwind wake extent from the largest LA cluster (LAs 1–7) is 14 km. It is associated with northwesterly flow scenarios (represented by simulations commencing on 1979-10-26 and 2007-02-05) (Figure 6A–6K). These simulations exhibit flow from over land to this LA cluster with relatively low freestream wind speeds (5–8 ms^{-1} at the center of these LAs at ~150 m in height) and moderate freestream TKE of ~1 m^2s^{-2}. The maximum wake extent from the LAs 1–7 of 90 km is found for the SW10-16 flow scenario (the simulation starting on 1986-03-26) and the NE4-10 flow scenario (represented by the simulation that starts on 2012-11-17) (Figure 6). The SW10-16 case exhibits higher wind speeds (freestream wind speed at ~150 m at the center of the LA cluster of ~10 ms^{-1}) but has a long over-water fetch, which results in low freestream TKE < 0.07 m^2s^{-2} that contributes to slow wake recovery and large wake-propagation distances. By contrast, the NE4-10 case exhibits higher TKE < 0.4 m^2s^{-2}, but lower wind speeds (WSs ~7.8 ms^{-1}) and higher thrust coefficients, which also lead to larger wake extents. For cases with southerly, southwesterly mean flow, i.e.,

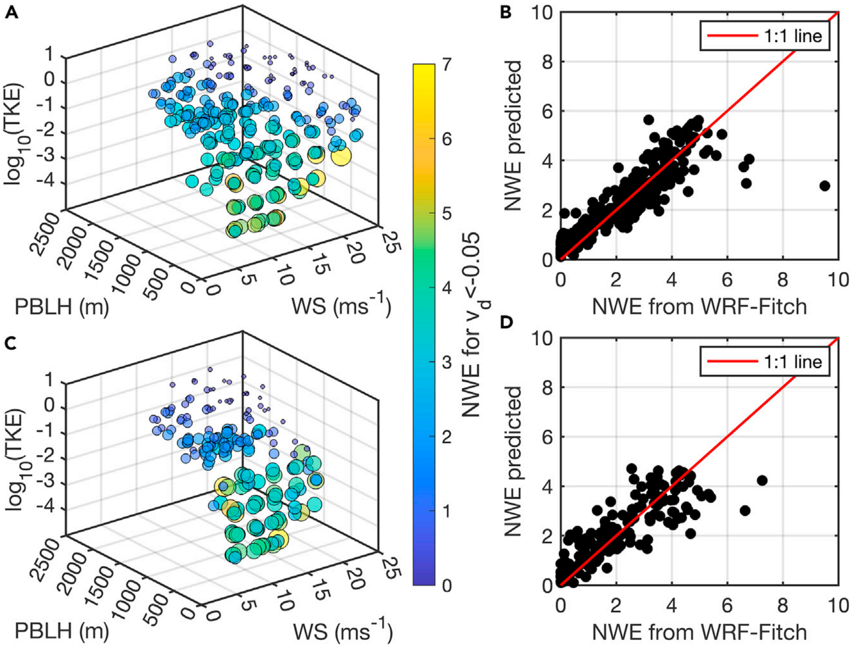

Figure 7. Spatial extent of disturbed flow (wakes) from offshore wind farms shown as a function of prevailing meteorology

(A and C) 3D bubble plots of the normalized wake extent (NWE, for a velocity deficit threshold 5%, i.e., $v_d < -0.05$) from each of the four lease-area clusters as a function of freestream wind speed (WS) and turbulent kinetic energy (TKE, shown in $\log_{10}$ scale) close to the wind-turbine HH of 150 m, and the freestream planetary boundary layer height (PBLH) in the centroid of the lease-area cluster.

(A) Results from the simulations of the control layouts, where wind turbines are installed with the mean separation of 7.7 times the wind-turbine rotor diameter. The installed capacity density for these control simulations is approximately 4.34 MWkm^{-2}.

(C) Results from the simulations of the half-density layouts, where the density of wind turbines is reduced to half that used in the control layout and represents the lowest densities used in European offshore wind farms. The associated installed capacity density is ~2.2 MWkm^{-2}.

(B and D) Scatterplots of the normalized wake extent (NWE) for each combined WS, PBLH, and TKE class derived directly from the WRF-Fitch output versus those predicted from the regression models.

(B) Results for an installed capacity density of 4.34 MWkm^{-2} (i.e., the control simulations) where the regression model has the form, $NWE = 3.52 - 0.093 \times WS - 0.73 \times log_{10}(TKE) - 6.3 \times 10^{-4} \times PBLH$.

(D) Results for an installed capacity density of ~2.2 MWkm^{-2} (i.e., the half-density simulations) where the regression model has the form, $NWE = 3.00 - 0.056 \times WS - 0.57 \times log_{10}(TKE) - 11 \times 10^{-4} \times PBLH$.

SW4-10 (1988-07-04), SW10-16 (1986-03-26), SW16-25 (1981-04-04) or northeasterly flow, NE4-10 (2012-11-17), velocity deficits above 5% fully encompass all of the mid-Atlantic LA clusters (LAs 9–13) indicating substantial array-array interactions, despite separation distances of up to ~23 km (Figure 6).

The SW4-10 flow scenario is observed for 12.5% of hours (Table 1) and is associated with the largest systemwide wake losses, and hence the smallest CFs (Table 1; Figure 4A). The 5-day simulation period starting 1988-07-04 has a freestream modal wind direction of ~210°, median WS of 6.3 ms^{-1}, and TKE below 0.01 m^2s^{-1} in LA 8. Mean CFs for LAs 1–7 for this flow scenario are particularly small (Figure 4B) due to low freestream WSs and a clear deep array wake effect. Fewer than 6% of wind turbines, all of which are located on the edge of the array, exhibit power production above 10% of rated power. Mean CFs for LAs 9–13 are also low for this flow scenario (14%) (Figure 4B), and the contour enclosing mean velocity deficits above 5% ($v_d \leq -0.05$) over the mid-Atlantic LA cluster for this flow scenario extends over a 210-km distance aligned along a south-southwest to north-northeast axis (Figure 6).

This variability in wake extents and CFs between the flow scenarios emphasizes the importance of simulating a wide array of atmospheric conditions and affirms the scenario construction used herein encompasses examples of maximum and minimum wake intensity and extent (Table 1). The composite overlay of areas with mean velocity deficits of over 5% (i.e., $v_d \leq -0.05$) under one or more of the flow scenarios (Figure 6L) provides important guidance for the selection of future LAs in order to avoid places with substantial wind shadowing from existing lease areas.

These thorough analyses of the power production and wake behavior across the different LA clusters along the U.S. east coast and their dependence on wind turbine layout and prevailing meteorology provides context that is critical to developing a generalized model for wind-farm wake extents that is presented in the next section.

A generalized model of wind farm wake extent

As illustrated in the previous discussion, the time or distance downstream required for a wind turbine wake to be eroded due to mixing with surrounding, higher-momentum air, is determined by the original intensity of the wake and the mixing state of the atmosphere. The wake intensity is, in large part, dictated by the freestream WS and the wind turbine thrust coefficient (Figure 1E). The mixing state of the atmosphere and ability to transfer higher-momentum air into the wake is determined by the ambient TKE and the planetary boundary layer height. Accordingly, the mean normalized spatial extent of wakes from each LA cluster scales primarily according to both mean freestream TKE and WS at HH (Figure 4C). Large, NWEs are most evident at low WSs and low TKE (Figure 4C). Conversely, for mean TKE above 0.5 m^2s^{-2}, the NWE is almost uniformly less than twice the area of the LA clusters (Figure 4C). A weaker but still important third control on wake extent is the planetary boundary layer height (Figure 7A).

Under the hypothesis that wind-farm intensity, areal extent, and recovery are largely controlled by three variables—freestream WS, TKE, and planetary boundary layer height—a generalized model of NWE is derived. The predictand is the NWE, i.e., the area covered by a mean velocity deficit [v_d] ≤ -0.05). The predictors are freestream WS, TKE, and planetary boundary layer height (PBLH) for the center of each LA cluster from the domain in which no wind turbine effects are simulated. Two models are derived (see details in methods). The first uses model output from simulations of the control layout that employ a wind turbine spacing equal to that agreed for some of the LAs and that typifies the European offshore wind energy industry (ICD of 4.34 $MWkm^{-2}$). The second model uses output from half-density layouts where the wind turbines are installed over the same area but with greater separation leading to an ICD of approximately 2.2 $MWkm^{-2}$. The NWE model for the control layouts has the following form:

$$NWE = 3.52 - 0.093 \times WS - 0.73 \times log_{10}(TKE) - 6.3 \times 10^{-4} \times PBLH \quad \text{(Equation 1)}$$

All of the coefficients are statistically different from zero at a confidence level of 99% and variance explanation (R^2), adjusted for the number of predictors,[45] is 0.72 (Figure 7).

The form of this linear model (Equation 1) indicates that the areal extent of the wake from a large offshore wind farm exhibits a statistically significant negative dependence on freestream WS close to the wind turbine HH, with larger wake generation at lower WSs. There is also a negative dependence on the base-10 logarithm of turbulence intensity ($\log_{10}$[TKE]) at wind turbine HH. Weaker ambient turbulence leads both to slower wake recovery and to larger wake extent. Both findings are consistent with analyses of operational data from offshore wind farms that have indicated below average power production, and larger wake effects, under moderate WSs and low turbulence intensity.[15] The model also indicates evidence of a negative dependence of NWE on freestream PBLH at the center of each LA cluster. For very large wind turbine arrays wake recovery is largely dictated by the rate at which momentum can be transferred from aloft. Mixing of high-momentum air from the free troposphere across the temperature inversion that typifies the top of the boundary layer into the boundary layer is very slow. Thus, under low PBLH the volume of air from which momentum can be extracted to recover the wake is smaller than under higher PBLH.

Using the half-density layout, the coefficients in the linear model are of the same sign for each of the predictors:

$$NWE = 3.00 - 0.056 \times WS - 0.57 \times log_{10}(TKE) - 11 \times 10^{-4} \times PBLH \quad \text{(Equation 2)}$$

Again, all of the coefficients are statistically different from zero at a confidence level of 99% and variance explanation (R^2), adjusted for the number of predictors,[45] is 0.70 (Figure 7).

The high variance explanation for Equations 1 and 2 indicate that these models are relatively good representations of the model output on which they are based. Further, there are robust relationships between the areal extent of a wake generated by very large offshore wind farms and the freestream WS and TKE near the wind turbine HH and the freestream PBLH. Consistent with expectations, for the same freestream WS, turbulence intensity, and PBLH the area covered by a wake from each wind farm is smaller for wind farms that have lower ICD, or greater wind turbine spacing. For example, for a WS of 7 ms^{-1}, TKE of 0.001 ms^{-2} and a PBLH of 500 m, the area covered by a 5% velocity deficit will be an average of 4.74 times the areal footprint of the wind farm if the wind turbines are installed with a spacing equal to that of current offshore wind farms in Europe. Conversely, for the half density of wind turbine deployments, the areal extent of the wind shadow is estimated to be 3.78 the area of the offshore wind farm.

In addition to demonstrating the functional dependence of wake extent on key meteorological drivers, these equations could provisionally be used with output from WRF simulations of other global regions to provide first-order estimates of likely wind shadows from proposed offshore wind farms. Naturally, caution should be used in extrapolating to atmospheric conditions beyond those sampled in this analysis and/or to scales of wind deployments dissimilar to those addressed here. Further, it is important to note that other modeling approaches are available to describe wind turbine and wind-farm wakes,[46,47] and different wind-farm parameterizations for use within the WRF model.[43] No assessment can currently be made regarding how results presented herein may differ from those generated using other modeling frameworks.

DISCUSSION

Expansion of offshore wind is a key component of global efforts to reduce the carbon intensity of the energy sector. Deeper understanding of the atmospheric physics of large wind farms is critical to optimal, cost-effective exploitation of the substantial offshore wind resource. Our research addresses this need and is unique in several regards. First, we present a computationally efficient and robust method to derive representative power production and wake projections for large offshore wind farms. Second, we demonstrate the approach and the concept of NWEs by applying our method to offshore wind LAs along that U.S. east coast. Last, we quantify the sensitivity of power production and wake-induced power losses to both wind-farm ICD and prevailing meteorology for a wide range of meteorological conditions that prevail offshore.

Our results indicate that power production of 116 TWh/year and mean CFs of ~ 50% can be achieved from the 15 U.S. east coast offshore wind energy LAs by employing 15-MW wind turbines at the anticipated spacing of 1.85 km (Table 1; Figure 4). CFs calculated for all three wind turbine layouts we considered meet or exceed those of currently operating offshore wind farms in Europe. They are consistent with, and indeed slightly higher than, those from an analogous WRF modeling study for projected installed wind energy capacity in 2050 for the German Bight region of the North Sea[6] (Figure 5). However, for wind turbine layouts similar to those from smaller offshore wind farms in Europe, a substantial fraction of these wind turbines will operate in wakes from upstream turbines and wind farms. These wake effects will reduce power production by over one-third (Figure 6; Table 1). There is clear evidence for substantial array-array interactions (i.e., power losses at downwind wind farms caused by wind turbines operating upwind) even for LAs separated by 23 km. These results emphasize the critical importance of evaluating potential wake losses from upstream wind farms as the BOEM moves forward with tendering additional LAs along the U.S. east coast.[36]

Using a low estimate of revenues from electricity production of $62 per MWh there are clear and substantial potential financial benefits from improved array layouts and careful siting of new wind turbine developments to reduce wake-induced power losses and increase CFs. At this scale of development (28.8 GW), a 1% increase in the CF would increase electricity output by about 2.5 TWh per year, leading to additional annual revenues of over US$150 million. Introduction of maritime corridors in the wind turbine layouts decreases estimated annual electrical-power production from 116 to 99 TWh/year. Thus, a reduction of total IC by 16.5% yields a reduction in projected power production of 14.7% because the increase in wind turbine spacing reduces wake-induced power losses and increases the efficiency of power production from the wind turbines. To provide an economic assessment of the maritime corridors scenario, we assume an installation cost of US$ 3 million per MW (the average of those projected for the U.S.[14] and realized in Germany[13]) and a power purchase price of US$ 62 per MWh of electricity produced (the average bid prices for European offshore wind farms[13]). Excluding any resulting additional cabling costs, introduction of the maritime corridors will decrease initial investment costs by ~US$ 14.3 billion but will also lower annual revenues by ~US$ 1.06 billion. Thus, the ultimate system-wide benefits of introducing maritime corridors and/or using higher or lower ICD merits detailed analyses, including all internal and external costs and benefits.

Projected power production, wake extent, and intensity are a nonlinear function of prevailing meteorology, e.g., wind resource and turbulence intensity (Figures 4C and 7), wind turbine layouts, e.g., ICD and areal extent (Figures 5 and 7), and model assumptions (e.g., wind-farm parameterization).[26,48,49] The statistical models developed here show the extent of wakes from large offshore wind farms can be explained by three atmospheric variables that are commonly available from meteorological models and/or can be measured using existing *in situ* and remote sensing technologies. The areal extent of disturbed flow normalized to the area of the wind farm that generates the wake is maximized under conditions of low turbulence intensity, moderate WSs, and low boundary layer heights (Figure 7). Thus, offshore wind farms are most likely to experience lower power production due to the presence of upstream wind farms under relatively low WSs and when warmer air moves over a colder sea. Under these conditions, the lower atmosphere will become stably stratified resulting in low ambient turbulence and low boundary layer heights.

Given the scale of the financial investment and the critical importance of offshore wind energy to the zero-carbon-emissions economy, further work is warranted. This should include a diversity of wind turbine layouts, inclusion of alternative windfarm parameterizations and additional atmospheric flow scenarios to ensure optimal design of individual offshore wind farms and management of the large-scale global expansion of offshore wind energy.

EXPERIMENTAL PROCEDURES

Resource availability

Lead contact

Requests for further information should be directed to the lead contact, Sara C. Pryor [redacted]

Materials availability

No materials were used in this study.

Data and code availability

Source code for WRF v3.8.1 including the wind-farm parameterization patch is available from [redacted]. ERA5 data are available from [redacted] Shapefiles of the lease areas are available from the BOEM at; [redacted] The population density in the contiguous U.S. according to the 2010 census is available from; https://www.census.gov/data/tables/time-series/demo/popest/2010s-state-total.html. Output from the WRF simulations presented in figures and analyses herein is available for download from ZENODO (10.5281/zenodo.5137547) access to the full suite of WRF output are available via the DoE tape archive. Output from simulations of the control layouts is available from: [redacted] Output from simulations of the layouts with maritime corridors is available from: [redacted] Output from simulations of the half-density layouts is available from: [redacted] MATLAB is a proprietary software program developed and available for purchase from MathWorks. MATLAB code used to perform the analyses is available for download from ZENODO (10.5281/zenodo.5137547).

Methods

Selecting the flow scenarios

The simulation and analysis framework presented here is designed to optimally quantify wake impacts on power production while reducing the computational cost and redundancy inherent in long-term continuous simulations. It further avoids limitations associated with use of idealized flow scenarios or individual case studies. The scenario approach ensures timely production of actionable information to those responsible for progressing development of offshore resources at the lowest LCoE. Details of the computational approach and costs are given in supplemental information.

The ERA5 reanalysis[50] is used to derive representative flow scenarios and the initial and lateral boundary conditions (LBC) for simulations with the WRF model. The ERA5 reanalysis model ingests an unprecedented suite of assimilated *in situ* and remote sensing observations.[50] ERA5 exhibits relatively high fidelity for 100-m wind speeds[40,51–53] and has been used as LBC in a range of WRF-based regional simulations including those performed for the New European Wind Atlas.[54] The periods for which WRF simulations are performed are selected based on analyses of WS and direction at 100 m a.g.l. for 1979–2018 from the ERA5 grid cell (30 × 30 km) containing the center of the New York LA (LA 8, Figures 1A and 1B). They are selected to represent commonly occurring flow conditions of relevance to power production and wake generation from wind turbines. Accordingly, the flow scenarios focus on the following WS classes; 4–10 ms^{-1} (high thrust coefficients causing relatively large wake magnitudes, Figure 1E), 10–16 ms^{-1} (moderate thrust coefficients and wakes) and 16–25 ms^{-1} (low thrust coefficients with small wake magnitude). The wind directions (WD) are also clustered into physically meaningful groups that represent differentiable modes of over-water fetch to the offshore LAs (Figure 2). Four directional classes are defined: 270°–360°, 180°–270°, 0°–90° and 90°–180° (listed in decreasing frequency). These directional classes represent flow that has a relatively short fetch over water to LA 8 (of the order tens rather than hundreds of km) for the two west sectors (SW: 180–270°, NW: 270–360°) versus those for the two easterly sectors (NE: 0–90°, SE: 90–180°) with hundreds to thousands of km of over-water fetch (Figures 1A and 1B). Ten combined WS and direction classes are required to capture 75% of the total 40 years of hourly observations. The flow scenarios are described using the nomenclature; WDWS, where WD is NE, SE, SW or NW, and WS is 4–10, 10–16 or 16–25.

Once the flow scenarios are identified, the 40 year record of hourly ERA5 derived WSs and directions at 100 m over the center of LA 8 is scanned to identify 5 day periods with the maximum number of hours that conform to each flow scenario (Table 1). Variation in atmospheric stability, turbulence intensity and PBLH offshore is dominated by the seasonal timescale due to the low frequency variability in sea surface temperatures.[55] Thus, in selecting the 5-day periods to represent the flow scenarios consideration is also given to ensuring the seasonal representation (Figure 2E). For the most frequent flow scenario (NW4-10), two cases; one in later autumn and one in summer are selected. Hence, 11 5-day periods are selected for the WRF model simulations (Table 1).

Simulation settings

Simulations are performed with WRF v3.8.1 and use the Fitch wind-farm parameterization.[38] This parameterization works such that every wind turbine in a grid cell contributes to estimated power production (in watts) as a function of the incident WS and the wind-turbine power curve (Figure 1E). Each wind turbine also induces wakes by applying a local drag force that reduces WSs and adds TKE to all model vertical levels that intersect the turbine rotor. Drag applied and TKE introduced are functions of the thrust coefficient (Figure 1E) and thus are determined by the incident WS and wind-turbine specifications.[38] Simulations performed here employ a modified version of the Fitch parameterization corrected for an earlier coding error that prevented advection of wind turbine induced TKE and that employs an updated algorithm for wind turbine added TKE.[37] Key physics setting are as in previous research[2] and shown in supplemental information. Each simulation employs a 6-h spin up and then runs for 5 days. All variables presented herein are output at 10-min intervals.

Wind resources and wind turbine wake effects are a function of model resolution.[26,48] Power density estimates from mesoscale models with a 10-km grid spacing can be 50% lower than those from higher-resolution modeling.[48] Here, four simulation domains are employed (Figure 1A). The outer domain comprises 150 × 150 grid cells with a grid resolution of 16.67 km (d01). This is nested down to the middle domain (d02) comprising 250 × 250 grid cells resolved at 5.56 km. Two inner domains of 340 × 361 grid cells resolved using a 1.85 km resolution are run sequentially. The first (d03) is operated without the action of wind turbines to provide a freestream WS. A second identical innermost domain (d04) is run with the wind-farm parameterization turned on. The resolution used for d03 and d04 is selected to match the expected wind-turbine separation of 1.85 km.

There are 57 layers in the vertical, 20 levels at which WSs are output are below 370 m and 14 are within the rotor plane. The nineth level has a mean height of 143 m and is taken as equivalent to that at the nominal wind turbine HH = 150 m (Figure 1D).

As of early 2021 wind-turbine selections and locations for the different U.S. offshore LAs are not available. Thus, simulations are performed for three plausible wind-farm layouts. The control employs a wind-turbine spacing of 1.85 km. For the IEA 15 MW reference turbine used herein has a HH ~ 150 m and a rotor diameter (D) ~ 240 m.[12] Thus, the spacing between wind turbine of 1.85 km is equal to a spacing of 7.7D. It is equal to the average wind-turbine spacing from operating wind farms in Europe. In this set of simulations all LAs are fully covered by a total of 1922 wind turbines (Figure 3). The mean wind turbine ICD for these control simulations is 4.34 $\mathrm{MWkm^{-2}}$. Two sets of sensitivity simulations are also performed for a subset of atmospheric flow conditions. In the corridor simulations, a maritime corridor is inserted by removing the sixth north-south "column" of wind turbines in each wind-turbine cluster, reducing the number of wind turbines to 1,604 (Figure 3). Such corridors have been proposed to accommodate shipping safety considerations and enable fishing,[56] and may also mitigate wildlife impacts.[57] In the half-density sensitivity simulations, the density of wind turbines in each LA is halved reducing the total number of wind turbines to 968. The resulting ICD (~2.1 $\mathrm{MWkm^{-2}}$) is at the lower end of current-generation European offshore wind farms.

Statistical methods

Power production reported here derives directly from the WRF wind-farm parametrization and is determined by the WS across the rotor plane and the wind-turbine power curve (Figure 1E).

Wind regimes in the LA clusters are compared by fitting time series of modeled freestream WS at the nominal wind-turbine HH of 150 m from the centroids of each LA cluster to a two-parameter Weibull distribution:

$$p(WS) = 1 - exp\left[-\left(\frac{WS}{A}\right)^{k}\right] \quad \text{(Equation 3)}$$

where the two parameters in this probability distribution are the scale parameter, A (units of $\mathrm{ms^{-1}}$) that describes the peak in the WS distribution and shape parameter, k, that describes the dispersion around that peak. These parameters are fitted using maximum likelihood methods.[45]

The wake intensity and spatial extent is characterized using the mean fractional velocity deficit (v_d) that describes the difference in WS due to the action of wind turbines. The mean v_d in each grid cell is computed using all output from each 5-day simulation (i.e., after the 6-h spin-up period is concluded) as:

$$v_d = \frac{1}{n}\sum_{i=1}^{i=n}\left[\frac{WS_{WT(x,y,i)} - WS_{NoWT(x,y,i)}}{WS_{NoWT(x,y,i)}}\right] \qquad \text{(Equation 4)}$$

The fractional velocity deficit is calculated using wind speeds at the wind-turbine HH using output from simulation domain d04 with the action of wind turbines included (WS_{WT}) and output from simulation domain d03 where no wind turbines are included (WS_{NoWT}). v_d is the mean of normalized difference in WS in each grid cell (x, y) at each of the 720 10-min timesteps in each 5-day period ($i = 1$ to $n = 720$). A two-sample t-test with a threshold p value of 0.01 is applied to assign statistical significance to the mean pairwise differences in WS. Results are corrected for multiplicity by ranking the p values from each grid cell (where $j = 1$ is allocated to the smallest p value and kk is the total number of grid cells) and then selecting as statistically significant only those for which the following condition is realized[45]:

$$p_j \leq \frac{j}{kk}p \qquad \text{(Equation 5)}$$

The concept of NWE is introduced to characterize the region of disturbed flow generated by a wind farm that is colloquially referred to as the "wind shadow." NWEs are calculated for each LA cluster in each 5-day simulation as the area covered by a mean $v_d \leq -0.05$ ($Area_{v_d \leq -0.05}$) divided by the spatial extent of the LA cluster (i.e., group of adjacent LAs, $Area_{LAcluster}$) that generates the wake:

$$NWE = \frac{Area_{v_d \leq -0.05}}{Area_{LAcluster}} \qquad \text{(Equation 6)}$$

The difference in NWE (ΔNWE) from each LA cluster in simulations with the control layout and the half-density layout is given by:

$$\Delta NWE = \frac{NWE_{control} - NWE_{half}}{NWE_{control}} \qquad \text{(Equation 7)}$$

Statistical models are constructed that describe the NWE, (i.e., the area covered by a 5% velocity deficit relative to the freestream WS normalized by the areal extent of the wind-turbine deployment) as a function of prevailing meteorology. Separate models are developed using output from the control layout simulations and using output from the half-density wind-farm layouts. In these analyses the NWE from each cluster of LAs is computed for each 10-min period along with the freestream WS, $\log_{10}$(TKE) and PBLH at the center of that LA cluster. To build stable regression models output from each LA cluster and each 10-min time stamp are first composited into combined classes of wind speed, turbulence and planetary boundary layer heights using seven WS classes (4–7, 7–10, 10–13, 13–16, 16–19, 19–22, 22–25 ms^{-1}), five $\log_{10}$(TKE) classes (5×10^{-5} to 5×10^{-4}, 5×10^{-4} to 5×10^{-3}, 5×10^{-3} to 5×10^{-2}, 5×10^{-2} to 5×10^{-1}, 5×10^{-1} to 5 m^2s^{-2}) and six PBLH classes (0–400, 400–800, 800–1,200, 1,200–1,600, 1,600–2,000, 2,000–2,400 m). The calculations are performed separately for each LA cluster (Figure 7) and then combined for the model generation. For each combined class of wind speed, turbulent kinetic energy and planetary boundary layer heights that has > 4 members, mean values of NWE, WS, $\log_{10}$(TKE) and PBLH are computed. The resulting regression equations describe NWE as a function of these predictors (see Figure 7). The regression coefficients are deemed statistically significant if they differ from zero at the 99% confidence level and the goodness of fit is evaluated using the R^2 value adjusted for the number of predictors.[45]

An estimate of wake-induced power production loss is made by computing the maximum possible power production in each 10-min period if each wind turbine experienced undisturbed flow. This estimate is derived by applying the IEA reference turbine power curve (Figure 1E) to freestream WSs from the third simulation domain (d03) at a model height of ~150 m in each grid cell where a wind turbine is present in simulation domain d04. The difference between the power derived using the wind-farm parameterization and this maximum possible power from the freestream WS is the wake loss:

$$wakeloss = \frac{\sum_1^{i=n}\left(\sum_{y=y1}^{y=y2}\sum_{x=x1}^{x=x2} PC\left(WS\left(x_{No_{WT}}, y_{NO_{WT}}, i\right)\right)\right) - \sum_1^{i=n}\left(\sum_{y=y1}^{y=y2}\sum_{x=x1}^{x=x2} P_{Fitch}(x_{WT}, y_{WT}, i)\right)}{n} \tag{Equation 8}$$

where I denotes the time stamps and ranges from 1 to n, where n = 720 for 10-min output over 5 days. PC is the power production as a function of WS computed from the power curve for the IEA 15 MW reference wind turbine (Figure 1E). P_{Fitch} is the power production from those same grid cells in simulation domain d04 computed by the modified Fitch scheme. The grid cells considered y1:y2 and x1:x2 are those that contain wind turbines in d04 for the control simulation.

SUPPLEMENTAL INFORMATION

Supplemental information can be found online at https://doi.org/10.1016/j.joule.2021.09.002.

ACKNOWLEDGMENTS

The US Department of Energy Office of Science (DE-SC0016605), the US Department of Energy Office of Energy Efficiency and Renewable Energy, and New York State Energy Research and Development Authority via the National Offshore Wind Research and Development consortium (147505) funded this research. This research was enabled by computational resources supported by the U.S. National Science Foundation via the Extreme Science and Engineering Discovery Environment (XSEDE) (award TG-ATM170024) and ACI-1541215, and those of the National Energy Research Scientific Computing Center, a DOE Office of Science User Facility supported by the Office of Science of the U.S. Department of Energy under contract no. DE-AC02-05CH11231. The comments from four reviewers are acknowledged.

AUTHOR CONTRIBUTIONS

S.C.P. and R.J.B. conceived the original concept and obtained the funding for the research. S.C.P. conducted all analyses presented here and drafted the manuscript and all figures. R.J.B. and S.C.P. designed the wind-turbine scenarios employed. R.J.B. designed the flow scenarios. T.J.S. performed the WRF simulations. S.C.P. and R.J.B. addressed review comments.

DECLARATION OF INTERESTS

The authors declare no competing interests.

Received: February 19, 2021
Revised: June 7, 2021
Accepted: September 8, 2021
Published: September 30, 2021

REFERENCES

1. Pryor, S.C., Barthelmie, R.J., Bukovsky, M.S., Leung, L.R., and Sakaguchi, K. (2020). Climate change impacts on wind power generation. Nat. Rev. Earth Environ. *1*, 627–643. [redacted]
2. Pryor, S.C., Barthelmie, R.J., and Shepherd, T.J. (2020). 20% of US electricity from wind will have limited impacts on system efficiency and regional climate. Sci. Rep. *10*, 541. [redacted]
3. Jacobson, M.Z., Delucchi, M.A., Bauer, Z.A.F., Goodman, S.C., Chapman, W.E., Cameron, M.A., Bozonnat, C., Chobadi, L., Clonts, H.A., Enevoldsen, P., et al. (2017). 100% clean and renewable wind, water, and

sunlight all-sector energy roadmaps for 139 countries of the world. Joule *1*, 108–121. [redacted]

4. He, G., Lin, J., Sifuentes, F., Liu, X., Abhyankar, N., and Phadke, A. (2020). Rapid cost decrease of renewables and storage accelerates the decarbonization of China's power system. Nat. Commun. *11*, 2486. [redacted]
5. HM Government. (2020). Energy white paper. Powering our net zero future. https://www.gov.uk/government/publications/energy-white-paper-powering-our-net-zero-future.
6. Engiewende, Agora, and Verkehrswende, Agora; Technical University of Denmark; max-planck-Institute for Biogeochemistry (2020). Making the most of offshore wind: re-evaluating the potential of offshore wind in the German North Sea. [redacted]
7. Musial, W., Heimiller, D., Beiter, P., Scott, G., and Draxl, C. (2016). Offshore wind energy resource assessment for the United States, p. 88, Technical report NREL/TP-5000-66599. [redacted]
8. EIA (2020). Electric power annual 2019 (Energy Information Administration). [redacted]
9. BOEM (2020). Coastal Virginia offshore wind project (CVOW) (United States Department of the Interior, Bureau of Ocean Energy Management). [redacted]
10. Barthelmie, R.J., Dantuono, K.E., Renner, E.J., Letson, F.L., and Pryor, S.C. (2021). Extreme wind and waves in U.S. east coast offshore wind energy lease areas. Energies *14*, 1053[redacted]
11. [redacted]
12. Gaertner, E., Rinker, J., Sethuraman, L., Zahle, F., Anderson, B., Barter, G.E., Abbas, N.J., Meng, F., Bortolotti, P., and Skrzypinski, W. (2020). IEA wind TCP Task 37: definition of the IEA 15-megawatt offshore reference wind turbine (National Renewable Energy Laboratory(NREL)). [redacted]
13. Jansen, M., Staffell, I., Kitzing, L., Quoilin, S., Wiggelinkhuizen, E., Bulder, B., Riepin, I., and Müsgens, F. (2020). Offshore wind competitiveness in mature markets without subsidy. Nat. Energy *5*, 614–622[redacted].
14. Stehly, T., Beiter, P., and Duffy, P. (2020). 2019 cost of wind energy review (National Renewable Energy Laboratory). [redacted]
15. Barthelmie, R.J., Hansen, K.S., and Pryor, S.C. (2013). Meteorological controls on wind turbine wakes. Proc. IEEE *101*, 1010–1019. [redacted]
16. Barthelmie, R.J., and Jensen, L.E. (2010). Evaluation of wind farm efficiency and wind turbine wakes at the Nysted offshore wind farm. Wind Energy *13*, 573–586. [redacted]
17. Thomsen, K., and Sørensen, P. (1999). Fatigue loads for wind turbines operating in wakes. J. Wind Eng. Ind. Aerodyn. *80*, 121–136. [redacted]
18. Veers, P., Dykes, K., Lantz, E., Barth, S., Bottasso, C.L., Carlson, O., Clifton, A., Green, J., Green, P., Holttinen, H., et al. (2019). Grand challenges in the science of wind energy. Science *366*, eaau2027. [redacted]
19. Lundquist, J.K., DuVivier, K.K., Kaffine, D., and Tomaszewski, J.M. (2019). Costs and consequences of wind turbine wake effects arising from uncoordinated wind energy development. Nat. Energy *4*, 26–34. [redacted]
20. Miller, L.M., Brunsell, N.A., Mechem, D.B., Gans, F., Monaghan, A.J., Vautard, R., Keith, D.W., and Kleidon, A. (2015). Two methods for estimating limits to large-scale wind power generation. Proc. Natl. Acad. Sci. USA *112*, 11169–11174. [redacted]
21. Miller, L.M., and Keith, D.W. (2018). Observation-based solar and wind power capacity factors and power densities. Environ. Res. Lett. *13*, 104008. [redacted]
22. Miller, L.M., and Keith, D.W. (2019). Corrigendum: observation-based solar and wind power capacity factors and power densities (2018 Environ. Res. Lett. 13 104008). Environ. Research Letters *14*, 079501. [redacted]
23. Hasager, C.B., Vincent, P., Badger, J., Badger, M., Di Bella, A., Peña, A., Husson, R., and Volker, P.J. (2015). Using satellite SAR to characterize the wind flow around offshore wind farms. Energies *8*, 5413–5439[redacted]
24. Platis, A., Siedersleben, S.K., Bange, J., Lampert, A., Bärfuss, K., Hankers, R., Cañadillas, B., Foreman, R., Schulz-Stellenfleth, J., Djath, B., et al. (2018). First in situ evidence of wakes in the far field behind offshore wind farms. Sci. Rep. *8*, 2163. [redacted]
25. Barthelmie, R.J., Pryor, S.C., Frandsen, S.T., Hansen, K.S., Schepers, J.G., Rados, K., Schlez, W., Neubert, A., Jensen, L.E., and Neckelmann, S. (2010). Quantifying the impact of wind turbine wakes on power output at offshore wind farms. J. Atmos. Oceanic Technol. *27*, 1302–1317. [redacted]
26. Pryor, S.C., Shepherd, T.J., Volker, P.J.H., Hahmann, A.N., and Barthelmie, R.J. (2020). "Wind theft" from onshore wind turbine arrays: sensitivity to wind farm parameterization and resolution. J. Appl. Meteorol. Climatol. *59*, 153–174. [redacted]
27. Wind Europe. (2020). Offshore Wind in Europe key trends and statistics (wind Europe). [redacted]
28. Mytilinou, V., and Kolios, A.J. (2019). Techno-economic optimisation of offshore wind farms based on life cycle cost analysis on the UK. Renew. Energy *132*, 439–454. [redacted]
29. Bosch, J., Staffell, I., and Hawkes, A.D. (2019). Global levelised cost of electricity from offshore wind. Energy *189*, 116357. [redacted]
30. Deutsche WindGuard. (2018). Capacity densities of European offshore wind farms. [redacted]
31. Enevoldsen, P., and Jacobson, M.Z. (2021). Data investigation of installed and output power densities of onshore and offshore wind turbines worldwide. Energy Sustain. Dev. *60*, 40–[redacted].
32. [redacted]
33. Nygaard, N.G. (2014). Wakes in very large wind farms and the effect of neighbouring wind farms. J. Phys.: Conf. Ser. *524*, 012162. [redacted]
34. Schneemann, J., Rott, A., Dörenkämper, M., Steinfeld, G., and Kühn, M. (2020). Cluster wakes impact on a far-distant offshore wind farm's power. Wind Energ. Sci. *5*, 29–49. [redacted]
35. Lee, J.C.Y., and Fields, M.J. (2021). An overview of wind-energy-production prediction bias, losses, and uncertainties. Wind Energ. Sci. *6*, 311–365. [redacted]
36. Boutwell, S. (2019). The path forward for offshore wind leasing on the outer continental shelf (Bureau of Ocean Energy Management), June 11, 2019. [redacted]
37. Archer, C.L., Wu, S., Ma, Y., and Jiménez, P.A. (2020). Two corrections for turbulent kinetic energy generated by wind farms in the WRF model. Mon. Weather Rev. *148*, 4823–4835. [redacted]
38. Fitch, A.C., Olson, J.B., Lundquist, J.K., Dudhia, J., Gupta, A.K., Michalakes, J., and Barstad, I. (2012). Local and mesoscale impacts of wind farms as parameterized in a mesoscale NWP model. Mon. Weather Rev. *140*, 3017–3038. [redacted]
39. Tammelin, B., Vihma, T., Atlaskin, E., Badger, J., Fortelius, C., Gregow, H., Horttanainen, M., Hyvönen, R., Kilpinen, J., Latikka, J., et al. (2013). Production of the Finnish wind atlas. Wind Energy *16*, 19–35. [redacted]
40. Pryor, S.C., Letson, F.W., and Barthelmie, R.J. (2020). Variability in wind energy generation across the contiguous United States. J. Appl.

Meteorol. Climatol. *59*, 2021–2039. [redacted]

41. Wind Europe. (2020). Wind Energy in Europe in 2019: Trends and Statistics. [redacted]

42. Ahsbahs, T., Maclaurin, G., Draxl, C., Jackson, C.R., Monaldo, F., and Badger, M. (2020). US East Coast synthetic aperture radar wind atlas for offshore wind energy. Wind Energ. Sci. *5*, 1191–1210. [redacted]

43. Volker, P.J.H., Badger, J., Hahmann, A.N., and Ott, S. (2015). The explicit wake parametrisation V1.0: a wind farm parametrisation in the mesoscale model WRF. Geosci. Model Dev. *8*, 3715–3731. [redacted]

44. Judge, F., McAuliffe, F.D., Sperstad, I.B., Chester, R., Flannery, B., Lynch, K., and Murphy, J. (2019). A lifecycle financial analysis model for offshore wind farms. Renew. Sustain. Energy Rev. *103*, 370–383. [redacted]

45. [redacted]

46. Sharma, V., Cortina, G., Margairaz, F., Parlange, M.B., and Calaf, M. (2018). Evolution of flow characteristics through finite-sized wind farms and influence of turbine arrangement. Renew. Energy *115*, 1196–1208. [redacted]

47. Wu, K.L., and Porté-Agel, F. (2017). Flow adjustment inside and around large finite-size wind farms. Energies *10*, 2164. [redacted]

48. Badger, J., and Volker, P.J.H. (2017). Efficient large-scale wind turbine deployment can meet global electricity generation needs. Proc. Natl. Acad. Sci. USA *114*, E8945 [redacted]

49. Volker, P.J.H., Hahmann, A.N., Badger, J., and Jørgensen, H.E. (2017). Prospects for generating electricity by large onshore and offshore wind farms. Environ. Res. Lett. *12*, 034022. [redacted]

50. Hersbach, H., Bell, B., Berrisford, P., Hirahara, S., Horányi, A., Muñoz-Sabater, J., Nicolas, J., Peubey, C., Radu, R., Schepers, D., et al. (2020). The ERA5 global reanalysis. QJR Meteorol. Soc. *146*, 1999–2049. [redacted]

51. Kalverla, P.C., Holtslag, A.A.M., Ronda, R.J., and Steeneveld, G.J. (2020). Quality of wind characteristics in recent wind atlases over the North Sea. QJR Meteorol. Soc. *146*, 1498–1515. [redacted]

52. Ramon, J., Lledó, L., Torralba, V., Soret, A., and Doblas-Reyes, F.J. (2019). What global reanalysis best represents near-surface winds? QJR Meteorol. Soc. *145*, 3236–3251. [redacted]

53. Jourdier, B. (2020). Evaluation of ERA5, MERRA-2, COSMO-REA6, NEWA and AROME to simulate wind power production over France. Adv. Sci. Res. *17*, 63–77. [redacted]

54. Hahmann, A.N., Sīle, T., Witha, B., Davis, N.N., Dörenkämper, M., Ezber, Y., García-Bustamante, E., González-Rouco, J.F., Navarro, J., Olsen, B.T., and Söderberg, S. (2020). The making of the new European wind atlas – part 1: model sensitivity. Geosci. Model Dev. *13*, 5053–5078. [redacted].

55. Barthelmie, R.J., Grisogono, B., and Pryor, S.C. (1996). Observations and simulations of diurnal cycles of near-surface wind speeds over land and sea. J. Geophys. Res. *101*, 21327–21337. 337. [redacted]

56. Mehdi, R.A., Schröder-Hinrichs, J.U., van Overloop, J., Nilsson, H., and Pålsson, J. (2018). Improving the coexistence of offshore wind farms and shipping: an international comparison of navigational risk assessment processes. WMU J. Marit. Affairs *17*, 397–434. [redacted]

57. Petruny, L.M., Wright, A.J., and Smith, C.E. (2014). Getting it right for the North Atlantic right whale (Eubalaenaglacialis): a last opportunity for effective marine spatial planning? Mar. Pollut. Bull. *85*, 24–32. [redacted]